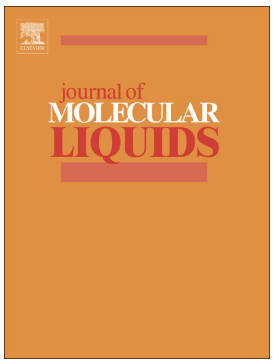

Development and optimization of a new hybrid chitosan-grafted graphene oxide/magnetic nanoparticle system for theranostic applications

M. Saviz Baktash, Ali Zarrabi, Ehsan Avazverdi, Nuno Miguel Reis

PII: S0167-7322(20)34904-7

DOI: https://doi.org/10.1016/j.molliq.2020.114515

Reference: MOLLIQ 114515

To appear in: *Journal of Molecular Liquids*

Received date: 27 July 2020

Revised date: 1 October 2020

Accepted date: 3 October 2020

Please cite this article as: M.S. Baktash, A. Zarrabi, E. Avazverdi, et al., Development and optimization of a new hybrid chitosan-grafted graphene oxide/magnetic nanoparticle system for theranostic applications, *Journal of Molecular Liquids* (2018), https://doi.org/10.1016/j.molliq.2020.114515

Development and Optimization of a New Hybrid Chitosan-grafted Graphene Oxide/Magnetic Nanoparticle System for Theranostic Applications

M. Saviz Baktash[1], Ali Zarrabi [1,2*], Ehsan Avazverdi[3], Nuno Miguel Reis[4]

[1] Department of Biotechnology, Faculty of Biological Science and Technology, University of Isfahan, Isfahan, Iran

[2] Sabanci University Nanotechnology Research and Application Center (SUNUM), Tuzla 34956, Istanbul, Turkey

[3] Department of Polymer Engineering and Color Technology (Tehran Polytechnic), No.350, Hafez Ave., Tehran, Iran

[4] Centre for Biosensors, Bioelectronics and Biodevices (C3Bio) and Department of Chemical Engineering, University of Bath, Claverton Down, Bath BA2 7AY, United Kingdom

* **Corresponding author, E-mail: alizarrabi@sabanciuniv.edu**
Tel: 0090 216 4839666, Fax: 0090 216 4839113

Abstract

There is currently a great demand especially in cancer treatment for transformative theranostic technologies combining imaging with drug delivery. This study reports the design and optimization of a hybrid theranostic nano-system combining the imaging capabilities of magnetic nanoparticles (MNPs) with the great potential of chitosan-grafted graphene oxide (GO) as a pH-sensitive smart nano-carrier. The grafting process was carried out in different molecular weights and concentrations of chitosan solution. Doxorubicin loading and release behavior, biocompatibility, and magnetic properties of the MNP/GO/chitosan nano-system were evaluated by different analytical methods. Increased pH resulted in a reduction in the rate of doxorubicin release, suggesting the formation of hydrogen bonds and the physical prevention of collapsed chitosan chains. In addition, a decrease in chitosan molecular weight, and an increase in concentration reduced the doxorubicin loading in around 24% yet a decrease in molecular weight increased the released amount in more than 200%. It can be related to fewer hydrogen binding and more contribution of π-π stacking in doxorubicin-chitosan interactions. The T2 contrast efficacy increased by grafting MNP/GO with high molecular weight chitosan due to the better surface coverage. Cytotoxicity assays with healthy L929 cell lines revealed high biocompatibility of MNP/GO/chitosan nano-system, suggesting chitosan prevents GO contact with the cell membrane. Further assays carried out with cancer cells MCF7 with MNP/GO/chitosan loaded with doxorubicin showed improved performance for MNP/GO grafted with low molecular weight chitosan. On the overall, the results indicated the hybrid MNP/GO grafted with high molecular weight chitosan at 6.0 g/dl showed the optimal properties for theranostic applications.

Keywords: Theranostic, Graphene oxide, Magnetic nanoparticles, Chitosan, Drug delivery.

1. Introduction

Cancer is a heterogeneous and adaptable disease, which is known as one of the most causes of human death in the world [1]. So far, many efforts have been conducted to identify an appropriate treatment manner for cancer also various methods were developed for that including surgery, chemotherapy, and radiotherapy. Surgery is the most comment approach for removing solid tumors, however it is very invasive and has limitations such as unpleasant condition for patients and hardly elimination of all tumor cells especially in the metastatic stages. Chemotherapy and radiotherapy present limited therapeutic effects, serious side effects on normal cells and adjacent tissues, and the risk of drug resistance. Thus, there is a major clinical need for novel engineering strategies for cancer treatment with reduced side effects, lower cost, and optimal therapeutic efficacy [2-6]. Minimally invasive strategies such as radio frequency ablation, microwave ablation, high intensity focused ultrasound, and irreversible electroporation are introduced as alternatives. These new strategies offer higher precision and patient tolerability in addition to lower side effects [7]. Despite of many attempts that have been made in this area; the 5-year survival of patients have not shown significant changed, with intensive research being conducted to overcome this critical issue [8].

Nanoparticles can easily travel all over the body through the bloodstream without being recognized by the immune system, permeate through the blood vessels, penetrate tissues, and deliver their cargo to the targeted cells [9-11]. The surface of these particles can be engineered with different polymers that not only improve their biocompatibility and blood circulation time, but also increase their drug loading and provide junction sites broad area for attachment of different factors like imaging or targeting agents [12-14].

The combination of imaging and therapeutic agents within a nanoparticle system introduces a new type of nano-system known as 'theranostic' which was coined by John Funkhouser for the first time in 2002[15].The use of theranostics for cancer open up potential application in cancer medicine which results to tailor a treatment regimen with improved outcomes, reduced costs, and fewer side effects along with the capability of monitoring the therapeutic efficacy during the treatment period lead to accelerate therapeutic decisions[16-17].

Common methods in tumor diagnosis include positron emission tomography (PET), computed tomography (CT), single photon emission computed tomography (SPECT), optical imaging (OI), ultrasound (US) and magnetic resonance imaging (MRI) [18].Due to its high spatial resolution, penetration depth and three-dimensional analysis, MRI has become one of the most popular diagnostic imaging techniques[19]. However, weak contrast between normal and cancerous tissues still restricts the application of this imaging technique in some patients. To address that issue, magnetic nano particles (MNPs) can be used as MRI contrast agents, these are currently commercialized under the tradenames of Resovist® or Feridex®; [20] however efforts to date have focused on increasing efficacy [32-35] and exploiting other applications [21-28].

The use of graphene oxide (GO) nano-sheets as drug carriers has received much attention in the last decade [29-31]. GO has been shown to improve the delivery of drugs, proteins and genes due to its particular properties including low toxicity, unique geometry, high loading capacity and

easy of synthesis [32]. In 2008, Dai et al. [33] introduced the first drug delivery system based on GO and demonstrated the application of polyethylene glycol/GO hybrid as a drug nano-carrier for loading of anti-cancer drugs via noncovalent bonding. Pramanik et al. [34] have recently reported the synthesis of GO-based magnetic nano-carrier using hyaluronic acid for delivering doxorubicin and paclitaxel and reported enhanced performance of GO/hyaluronic acid system comparing with pristine GO in targeting and killing CD44-expressing breast cancer cells.

Chitosan is a form of linear cationic polysaccharides with natural origins that has numerous biological applications in drug and gene delivery and tissue engineering which shows desired properties include biocompatibility, biodegradability, and anti-bacterial activity [35-37].This is a type of smart polymer which can respond to the environmental stimulus, as solubility varies reversibly by changing pH value. In addition, the high density of hydroxyl, ether and amine functional groups in the structure of chitosan suggests this is an ideal candidate for modifying GO[38].The non-covalent method is widely used for modification of GO by chitosan to be used as a drug carrying system[39-40]. It was also shown that GO/chitosan physical interactions can be affected by the pH of the environment so that the dispersion state can be changed from well-dispersed to agglomerated depending on the pH of the system[41].Although the physical interaction is a simple tool to achieve homogeneous GO/chitosan suspension, covalent bonding leads to the formation of a novel hybrid system which represents the properties of both components[42].

This manuscript reports functionalization of magnetic graphene nano-sheets with chitosan to be used as a nano-theranostic system. In particular, it explores in detail the effect of chitosan molecular weight and chitosan concentration on its grafting density onto GO in respect to drug release, biocompatibility and magnetic behavior of the system, which to the best of our knowledge has not previously been reported in literature yet essential to fully demonstrate the theranostic potential of graphene nano-sheets.

2. Materials and Methods

2.1 Materials

High, medium and low molecular weight chitosan with 75-85% deacetylation degree, reaction-grade graphite powder and Dimethylsulfoxide (DMSO) were all sourced from Sigma-Aldrich (St. Louis, USA). Acetic acid, sulfuric acid, sodium nitrate, potassium permanganate, hydrogen peroxide, sodium hydroxide, ethyl (dimethyl amino propyl) carbodiimide (EDC), N-Hydroxy succinimide (NHS), iron (III) chloride, and iron (II) sulfate were all obtained from Merck Millipore (Frankfurter, Germany). 3-(4,5-dimethylthiazol-2-yl)-2,5-diphenyl tetrazolium bromide (MTT) powder, phosphate buffer saline (PBS) and fetal bovine serum (FBS) were purchased from Gibco and Penicillin /Streptomycin from BioIdia. MCF-7 human breast cancer and L-929 mouse fibroblast cells were sourced from the Pasteur Institute of Iran.

2.2 Fabrication of GO Nanoparticles

The modified Hummers method was employed to fabricate GO[3]. Briefly, 115 ml of H_2SO_4, 5 gr graphite powder and 2.5 gr $NaNO_3$ were stirred in an ice-bath for 30 minutes. After that, solution of KMnO4 was added dropwise to the above mixture through 2 h. Deionized water was slowly added to the mixture and stirred at 35°C for 3 h. 50 ml 30 wt. % H_2O_2 solution was added to the mixture followed by 30 minutes whilst stirring at 98°C. Finally, the oxidized sample was washed three times with a solution of 10 wt. % HCl in deionized water in a 37 kHz ultrasonic bath with the power of 90 W (S10H model, Elma Schmidbauer GmbH, Singen, Germany). The pH value of the suspension was increased to 6 by washing several times the resultant GO with deionized water after centrifuging. Following completion of the reduction, the mixture was cooled to room temperature and then 1.2 g NaOH and 1g chloroacetic acid added to the mixture and placed in the ultra-sonic bath for 3 h to obtain GO-COOH. Then the mixture was centrifuge at 6,000 rpm for 30 minutes for 5 times to reach pure GO-COOH. Finally, the GO-COOH was dried with freeze drier (Alpha 1-2 LD plus, Christ, Osterode Germany) [43].

2.3 Fabrication of Magnetic GO Nanoparticles

MNPs were first prepared by dissolving 11.02 M of $FeCl_3.6H_2O$ and 5.06 M of $FeCl_2.4H_2O$ in 150 ml deionized water at 50°C for 2 h to achieve an orange-colored solution. 20 ml Ammonia was added drop wise to this solution in 30 minutes under nitrogen atmosphere. Then, in order to precipitate MNPs on GO, MNPs were first dispersed in a 1 molar nitric acid solution for one hour. GO was placed in an ultrasonic bath for 1 h to be suitably dispersed. Eventually, the required amounts of MNP suspension were mixed with GO solution for 5 h. The final products were precipitate by magnet and washed with deionized water to remove the non-interacted GOs. Then non-interacted MNPs were also separated by means of centrifuging (Universal 320 model, Hettich, Germany) at 400 rpm [44].

2.4 Chitosan Grafting

A mixture of 3 mg of GO-COOH/MNP in 1 ml water was activated with EDC (53.7 mg) and NHS (55.3 mg) for 30 min and then added to a chitosan solution with different molecular weight and concentrations and stirred for 4 h at room temperature. At the end, the nano system was centrifuged and re-suspended in acetic acid 1% v/v and washed for 5 time to ensure removal of free chitosan.[54] The samples formulations were shown in **Table 1**. Synthesis path of the theranostic system in this study is shown in **Scheme 1**. Concentrations of chitosan solutions were chosen in the range of dilute ($C<C^*$), semi-dilute ($C^*<C<C^{**}$), and concentrated ($C^{**}<C$) regimes. Critical concentrations (C* and C**) for the chitosan solution were measured based on rheological assessments which are described in the **Supplementary Information.**

Table 1: Materials and formulations contributed in samples.

Code	Molecular weight	Concentration (g/dl)	MNP:GO
H0.5-1:1	High	0.5	1:1
H2-1:1	High	2	1:1
H6-1:1	High	6	1:1
M0.5-1:1	Medium	0.5	1:1
M2-1:1	Medium	2	1:1
M6-1:1	Medium	6	1:1
L0.5-1:1	Low	0.5	1:1
L2-1:1	Low	2	1:1
L6-1:1	Low	6	1:1

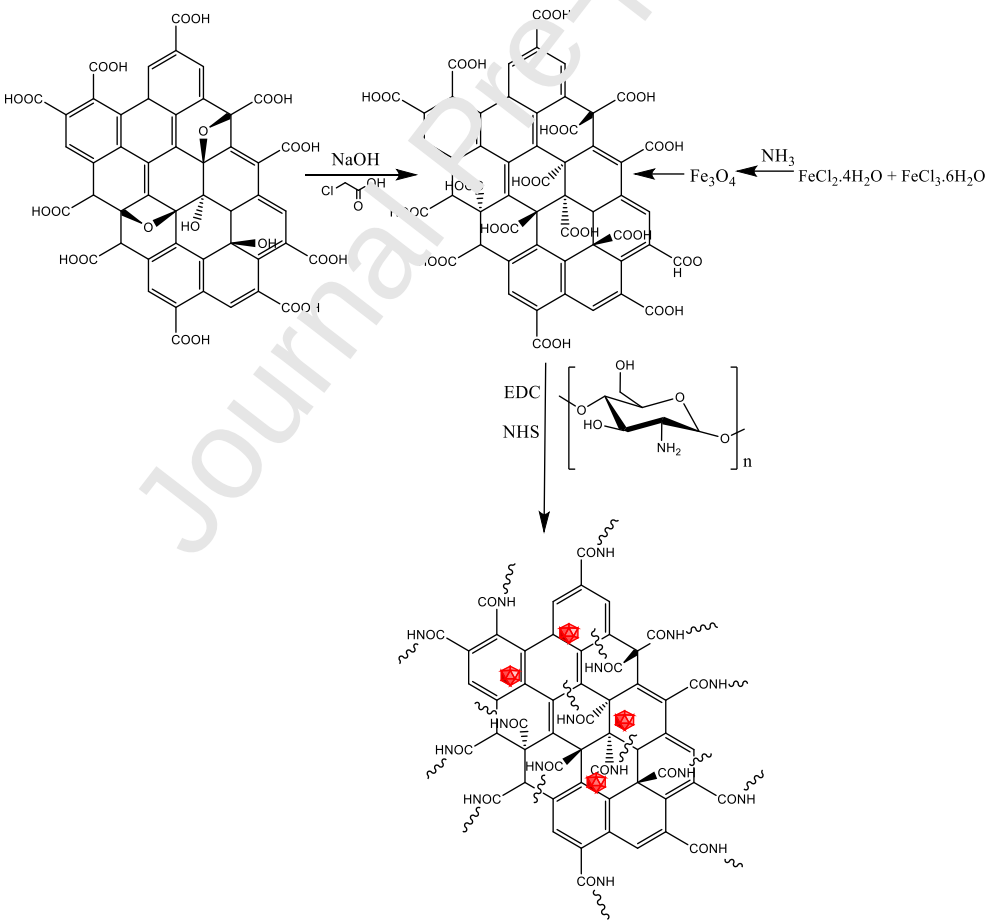

Scheme 1. Production of GO-COOH, MNP/GO and MNP/GO/chitosan system.

2.5 Characterization

X-ray diffraction (XRD) patterns of GO nanoparticles were measured by X'Pert diffractometer instrument (Philips, Amsterdam, Netherland, with a Cu-Kα anode). The d-spacing of graphite and GO was calculated using the Bragg's law. Fourier transfer infrared (FTIR) spectra of the samples were recorded in the wave number range of 400-4000 cm^{-1} using MB-100 spectrometer (ABB Bomem, Zurich, Switzerland). Thermo gravimetric analyses (TGA) of the samples were performed in the range of 25-700°C at heating rate of 10°C/min (Mettler Toledo, Columbus, USA). The magnetic properties of the samples were evaluated via vibrating sample magnetometer (VSM) (Lakeshore 7307, Carson, USA) at ambient temperature.

2.6 Drug Loading and Kinetics of Release

Drug loading tests were performed by the addition of 5 mg of the as synthesized delivery nano-system to 10 ml of the 2 mg/ml doxorubicin solution, followed by 8 h mixing at 4°C. After that, the nanoparticles were separated from the solution through centrifuging at 8,000 rpm. Unloaded drug was measured by UV-Vis spectroscopy (UV-1601PC, Shimadzu, Kyoto, Japan) at 485 nm and the total drug loading (expressed in percentage) was calculated using the following equation [45-46] :

$$Drug\ loading(\%) = \frac{Mass\ of\ loaded\ DOX}{Mass\ of\ nanoparticles} \times 100 \quad (1)$$

Kinetics of doxorubicin release were performed by pouring 2 ml of 1 mg/ml drug-loaded nano-system in a dialysis bag and placing in 5 ml phosphate buffer of pH=7.4 and 5.1, corresponding to the pH of biological fluid and lysosome, respectively [47-49]. The temperature was kept constant at 37°C. The total PBS was replaced with fresh one at different time intervals (2, 4, 6, 18, 30, 42, 54h). The amount of the drug released was evaluated at 485 nm wavelength using UV-Vis spectrometry [46] and expressed as:

$$m(t_n) = \sum_{i=1}^{n} C(t_i)V \quad (2)$$

$$Cummulative\ release = \frac{m(t_n)}{m_0} \quad (3)$$

where $m(t_n)$ is mass of released drug at n^{th} time point; C is the concentration of the drug in the buffer; V is the volume of the buffer; and m_0 is the mass of loaded drug in the nano-system.

2.7 Cell Viability Studies

MTT assay was used to assess the cytotoxicity of the nano-systems. For this, MCF7 and L929 cell lines were chosen as the cancerous and normal cell lines, respectively. For the L929 cell line the procedure started by culturing around 10,000 cells in each well of a 96 well microwell plate for 24 h at 37 ˚C with 5% CO_2, after which the cell culturing media was replaced by fresh media containing different concentrations of nanoparticles (25, 50 and 100 µg/ml). The effect on the viability of the cells was assessed after 24, 48 and 72 h using MTT. For this, the medium of each well was removed, and cells washed twice with PBS buffer. Then, cells were loaded with 10 µl of MTT solution (5 mg/ml) in 100 µl of pure media for about 4 h at 37 ˚C and the medium replaced by 100 µl of DMSO. After 1 h incubation the absorbance of each well was measured at 490 nm with a microplate reader (ELx800, Biotek, Winooski, USA) [46,50]. For MCF7 cell line above procedure was repeated with different concentration of aliquot drug loaded nanoparticles (1, 2, and 4 µg/ml of loaded doxorubicin)

2.8 Magnetic Resonance Imaging

MRI experiments were carried out at 25°C using a magnetic resonance (MR) scanner (GE Healthcare, Signa Explorer 1.5T, USA). To evaluate T_1 and T_2 effects in an aqueous solution, the nano-system were dispersed in water (10 ml) with different MNP concentrations at 0, 25, 50, 100, 200 and 400, µmol/l Fe, respectively. The sample tubes were placed into the MR scanner and 8 number of spin-echo sequences were run for obtaining both T_2 and T_1 relaxation times. The GE media viewer software was used for data acquisition. To estimate the T_2 relaxation time for each sample, coronal images (*TH* = 10 mm) were acquired at various echo times (*TE*) from 10 to 150 ms with a repetition time (*TR*) of 1600 ms. Similarly, the T_1 relaxation time for each sample was measured by varying *TR* between 100 and 6400 ms while keeping *TE* constant at 18 ms. After acquiring the images, the magnitudes of image intensities were analyzed within manually drawn regions of interest (ROIs) with a constant area for each sample. Relaxation rates R_1 ($1/T_1$) and R_2 ($1/T_2$) were calculated by mono-exponential curve fitting of the signal intensity vs. time (*TE* or *TR*). Equations 2 and 3 were used for curve fitting of relaxation rate R_1 and R_2, respectively [51]:

For relaxation rate R_1:

$$I = A.[1 - exp(-R_1.TR)] \quad (4)$$

For relaxation rate R_2:

$$I = A + C.[exp(-R_2.TE)] \quad (5)$$

2.9 Statistical Analysis

All data was analyzed with Minitab 17 statistical software using one-way analysis of variance (ANOVA). Pairwise comparisons were performed using Tukey's test. α value was equal to 0.05 and p-values less than 0.05 were considered statistically significant.

3. Results and Discussion

3.1 Synthesis of GO Nanoparticle

XRD patterns of the pristine graphite and synthesized GO nanosheets are illustrated in **Fig. 1.** The strong peak of graphite located at 2θ=26.8° disappeared in the spectrum of GO nanosheets. GO characteristic peak was observed at 2θ=11.8°. The peak location change is associated with the broadening of peak and severe drop in its intensity. Stobinski [52] and Park [53] attributed this to the presence of oxygen reached functional groups and water molecules in the galleries of the GO comparing with the pristine graphite.

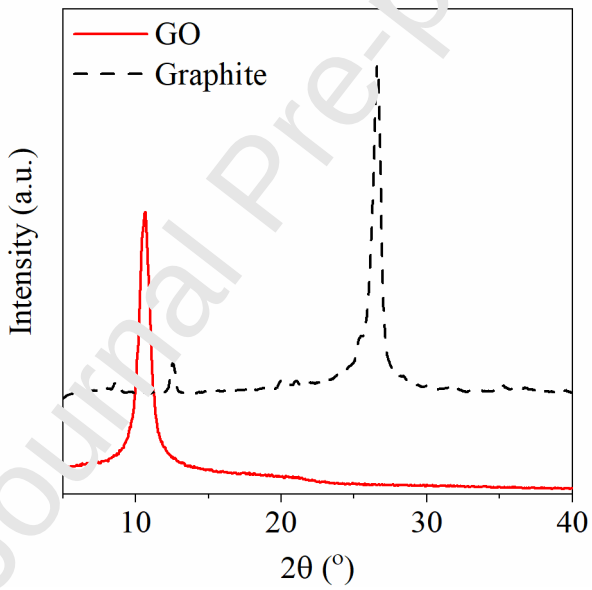

Fig. 1. XRD patterns of the initial graphite (black) and synthesized GO nanosheets according to the modified Hummers method (red).

3.2 Characterization of the Synthesized Delivery Nano-Systems

FTIR spectra for MNPs, GO, MNP/GO, chitosan, L2-1:1 and H2-1:1 nano-systems were summarized in **Fig. 2-A**. The MNP spectrum shows two broad peaks at 579 and 3450 cm^{-1} which are attributed to Fe-O and O-H stretch vibration, respectively. For GO two characteristics peaks at 1160 and 1730 cm^{-1} were related to C-O-C epoxide asymmetric bending and C=O stretching of carboxylic acid group, respectively. Appearance of a sharp peak at 579 and 1160 cm^{-1} and a weak peak at 1730 cm^{-1} in MNP/GO spectrum depicts that the MNPs were interacted with the

GO nanosheets. Chitosan characteristic peaks appeared at 1620 cm^{-1} (bending vibration of N-H in NH_2), 2880 cm^{-1} (stretching vibration of C-H), 3450 cm^{-1} (O-H stretching), and 1160 cm^{-1} (C-O-C glucose ring ether) [54]. The appearance of chitosan peaks at around 1620, 2880 and 3450 cm^{-1} in the synthesized nano-systems (e.g. L2-1:1 and H2-1:1 in **Fig. 2A**) confirmed successful grafting of chitosan on GO surface.

TGA analysis was performed to investigate the effect of molecular weight on chitosan grafting onto the surface of the nano-carriers. Mass losses of the MNPs, GO, MNP/GO chitosan and systems synthesized with various molecular weights of chitosan (with constant concentration) were illustrated as a function of temperature (**Fig. 2-B)**. Both GO and MNPs possess high thermal stability so that their weight loss in the range of 100 to 600 °C were 20% and 3%, respectively, which are due to the presence of carboxylic acid and hydroxyl groups on the surface of GO and MNPs. For samples containing chitosan two major weight loss in the temperature ranges of 50-100 °C and 260-380°C have been observed which are attributed to the water elimination and pyroelectric degradation as well as the elimination of oxygen and nitrogen, respectively[55]. By grafting different molecular weight of chitosan on the GO surface, the weight loss of the samples was intensified in the range of 50-100°C, suggesting more water absorption by the nano-systems grafted with higher molecular weight chitosan. The onset temperature of pyrolytic degradation was reduced from 300°C for pure chitosan down to 260°C for chitosan-grafted samples which can be attributed to the overlap of the pyrolytic degradation peaks of GO (120°) and chitosan (260°C)[56].

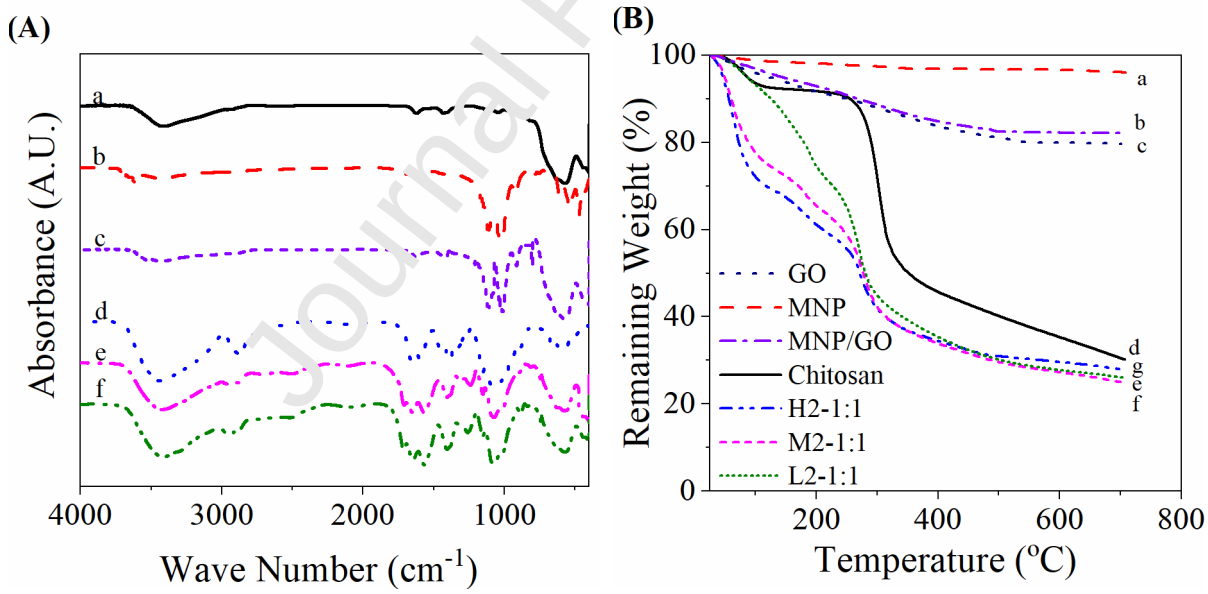

Fig. 2. (A): FTIR spectra of MNP (a), GO (b), MNP/GO (c) chitosan (d), L2-1:1 (e) and H2-1:1 (f). (B): TGA diagrams of magnetic nanoparticles (a), MNP/GO (b), GO (c), chitosan (d), and samples L2-1:1 (e), M2-1:1 (f) and H2-1:1 (g) in the range of 25-700°C.

3.3 Drug Loading Efficiency of the GO/Chitosan/Magnetic Nano-Delivery System

The effect of chitosan concentration and molecular weight on the efficiency of doxorubicin loading was represented in **Fig. 3** for the MNP/GO/chitosan nano-system synthesized with different molecular weights and concentration regimes (**Fig.S1** and **Table S1**). The amount of drug loading at concentration of 2% was lower than that for 0.5 and 6%, suggesting drug loading is very dependent on the concentration of grafting chitosan. Moreover, the use of higher molecular weight chitosan helped improving up to 24% the drug loading efficiency compared to medium and low-molecular weight. For MNP/GO systems synthesized in the in high molecular weight chitosan solution and high concentration (above C** - see rheological data in supplementary material), the abundance of polymer chains caused formation of a dense layer of chitosan branches on the GO surface. Hence, upon completion of reaction, the modified nano-system presented a structure with a high number of chitosan chains, which disturbed π-π stacking interactions but enhanced hydrogen binding by means of large number of glucosamines repeating units. However, in systems synthesized in low concentrations of high molecular weight chitosan solution, a sparse graft of chitosan chains formed on the GO surface and doxorubicin absorption mostly took place via π-π stacking[57].Whilst in semi-diluted systems chitosan covered higher surface area of the GO, it did not grafted chains as much as the concentrated solution, therefore π-π stacking was disturbed by chitosan chains while their number was not high enough to absorb equivalent doxorubicin through hydrogen bonding mechanism. For the systems with medium molecular weight the number of chains on the GO surface was high enough to disturb the π-π stacking interactions but not high enough to form sufficient hydrogen bonding interaction sites due to fewer glucosamine repeating units; therefore, it showed lower doxorubicin loading than at other concentrations. The drug loading change with concentration for the medium molecular weight chitosan was not significant, statistically. The system synthesized with low molecular weight chitosan cannot absorb doxorubicin through hydrogen binding as much as high molecular weight chitosan due to the lower number of repeating units. Increasing the concentration in low molecular weight systems leads to higher drug loadings.

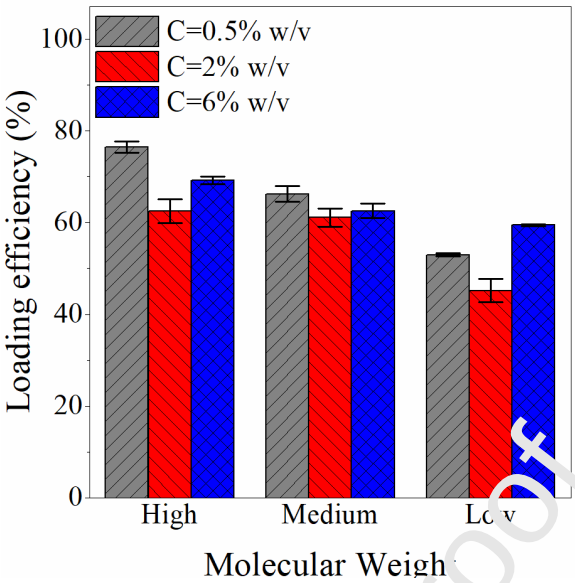

Fig. 3. Drug loading in MNP/GO/chitosan nano-systems for three types of low, middle and high molecular weight of chitosan at 0.5, 2 and 6% w/v concentrations.

3.4 Kinetics of Doxorubicin Release

Considering the higher efficiency of drug loading with the MNP/GO grafted with high molecular weight chitosan, the next experimental set aimed at testing the effect of pH on the kinetics of drug release. The rate of drug release was in general faster at pH=5.1 compared to pH=7.4 as shown in **Figs 4-A.** The initial burst rate of release followed the same trend. The absorption and desorption of doxorubicin on the GO surface is known to be governed by two basic interactions[50]: a) π-π interaction between the aromatic rings of doxorubicin and conjugated graphitic bonds of GO, and b) the hydrogen bonding of hydroxyl and amine groups in doxorubicin with hydroxyl and carboxyl functional groups on GO and hydroxyl and amine functional groups of chitosan. At neutral pH, a strong hydrogen bond forms between GO and doxorubicin whilst in acidic pH it is weakened, and doxorubicin desorption can easily take place. As expected, the MNP/GO grafted with high molecular weight chitosan has more potential sites for hydrogen bonding therefore showing severe differences in the doxorubicin release profiles. On the other hand, the presence of chitosan on the GO surface retards the doxorubicin desorption by exposing more hydrogen bonding and spatial hindrance. Upon increase of pH, the solubility of chitosan is decreased, and the chitosan chains transform from the swollen to collapsed state, therefore, the drug is entrapped between collapsed chitosan chain with the initial rate of release significantly decreasing[58].At pH=5.1, with the chitosan chains being in the swollen state, the drug releases more easily with contact with PBS buffer. This behavior was more pronounced at 2 and 6% w/v concentrations than 0.5% w/v (**Fig. 4-A**). This is believed to be due to the diluted concentration being insufficient to fully cover the MNP/GO surface with the chitosan. At such low concentration, doxorubicin desorption was less affected by chitosan hydrogen bonding and conformational state of the chain in comparison with MNP/GO grafted in the high concentration chitosan solution.

An additional set of experiments showed a considerable increase in both the initial rate and total amount of doxorubicin released upon using low molecular weight chitosan (**Fig. 4 B-D**). Low molecular weight chitosan means less glucosamine units were available to interact with doxorubicin, which enhances the contribution of π-π stacking; therefore, the most important factor retarding doxorubicin release was eliminated and release was accelerated. As the molecular weight of chitosan is increased at low concentrations, the number of hydrogen bonds between chitosan and doxorubicin is increased slowing down the rate of drug release. The release profile for 2% w/v samples did not show any significant changes.

With the use of higher concentration of chitosan (6 g/dl, **Fig. 4-D**), the use of low molecular weight chitosan yielded a remarkable increase on both burst release and total amount of doxorubicin release, suggesting the rate of drug release can be decreased by increasing the R_h and number of the polymer functionalities as suggested[59].

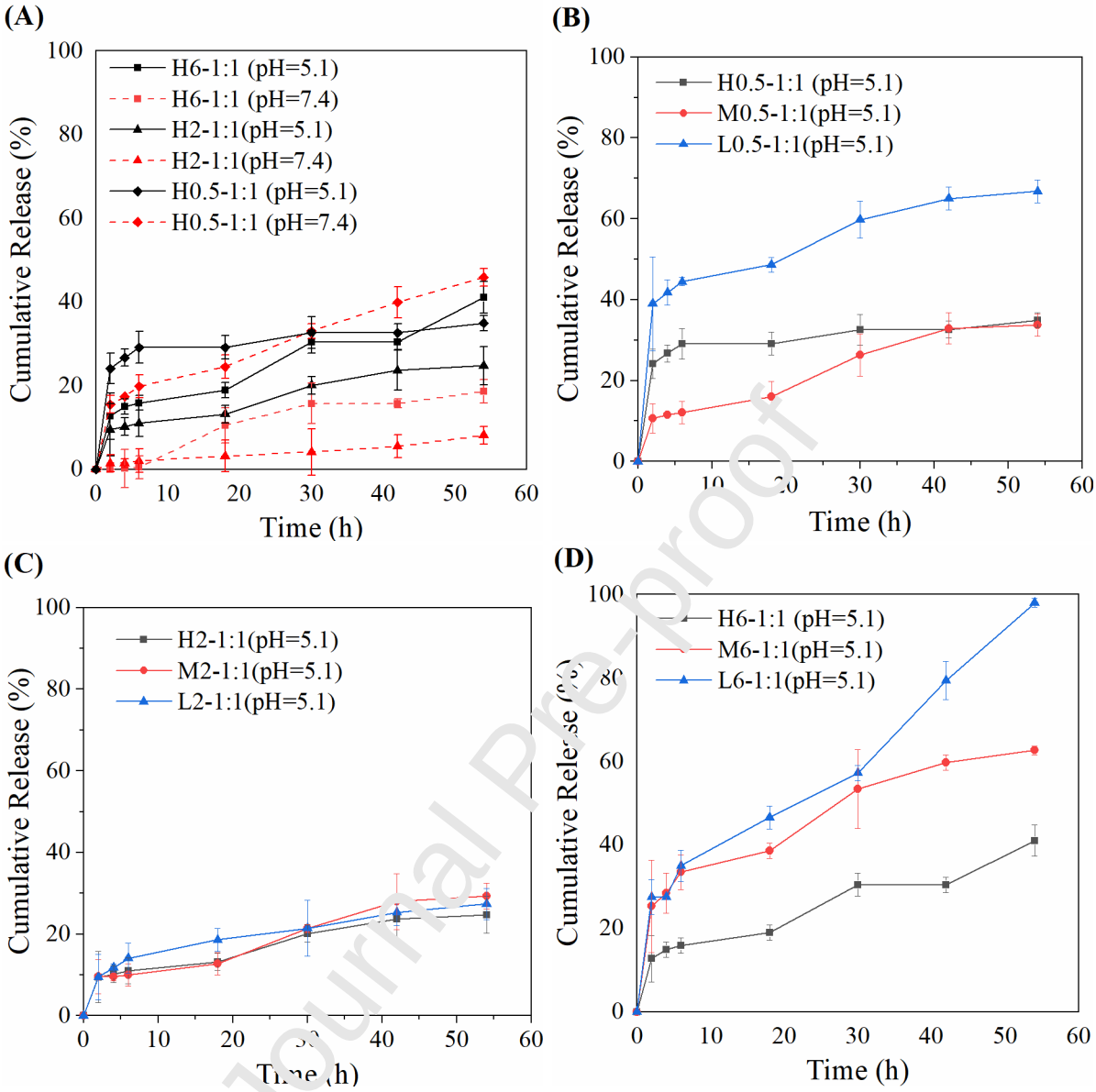

Fig. 4. Drug release profile from nano-systems containing (A): high molecular weight chitosan synthesized in different concentrations at 5.1 and 7.4 pH values and (B-D): chitosan with different molecular weights synthesized in concentration of 0.5, 2 and 6g/dl respectively at pH=5.1

3.5 Cell Viability and Toxicity

Toxicity tests with healthy L-929 fibroblast cells exposed MNP/GO nano-carriers showed about 77% cell survival for cells exposed to uncoated MNP/GO (**Fig. 5-A**), which can be due to intracellular penetration and the rupture of cellular membrane previously reported for GO[60]. In contrast, the chitosan grafted MNP/GO showed negligible cell death. As the molecular weight of chitosan increased, the cellular compatibility also increases. An increase on molecular weight yields higher electrostatic and spatial repulsion between chitosan chains and the cell membrane,

hence decreasing the probability of direct GO contact with the cell membrane, therefore cell survival increased by increasing the molecular weight. Experiments at higher and lower concentration of chitosan showed the grafting of MNP/GO with high molecular weight chitosan does not show considerable decrease in the cellular toxicity of the system in the wide range of concentration (**Fig. 5-B**) comparing with systems grafted with lower molecular weight chitosan. These results are in good agreement with other works [61].

Cell cytotoxicity of MCF7 cancer cells was also tested using MNP/GO/chitosan nano-systems containing 1, 2 and 4 μg/ml of aliquot doxorubicin (**Fig. 5-C**). Free doxorubicin with the same concentrations and drug free cell culture environment were used as the positive and negative controls, respectively. Naturally, cell viability reduced by increasing the concentration of the drug and in general all chitosan-grafted MNP/GO systems showed a reduction in cell viability similar to doxorubicin in solution, overall with low molecular weight outperforming the medium and high molecular weight chitosan samples by 38.5±1.8 % MCF7 viability. This is attributed to higher percentage of drug release due to the increase of π-π stacks formation between doxorubicin and GO, as discussed previously. In samples with medium and high molecular weight chitosan, the presence of more chitosan/doxorubicin interaction site decelerates the doxorubicin release, leading to decrease in their cytotoxicity comparing with the low molecular weight sample.

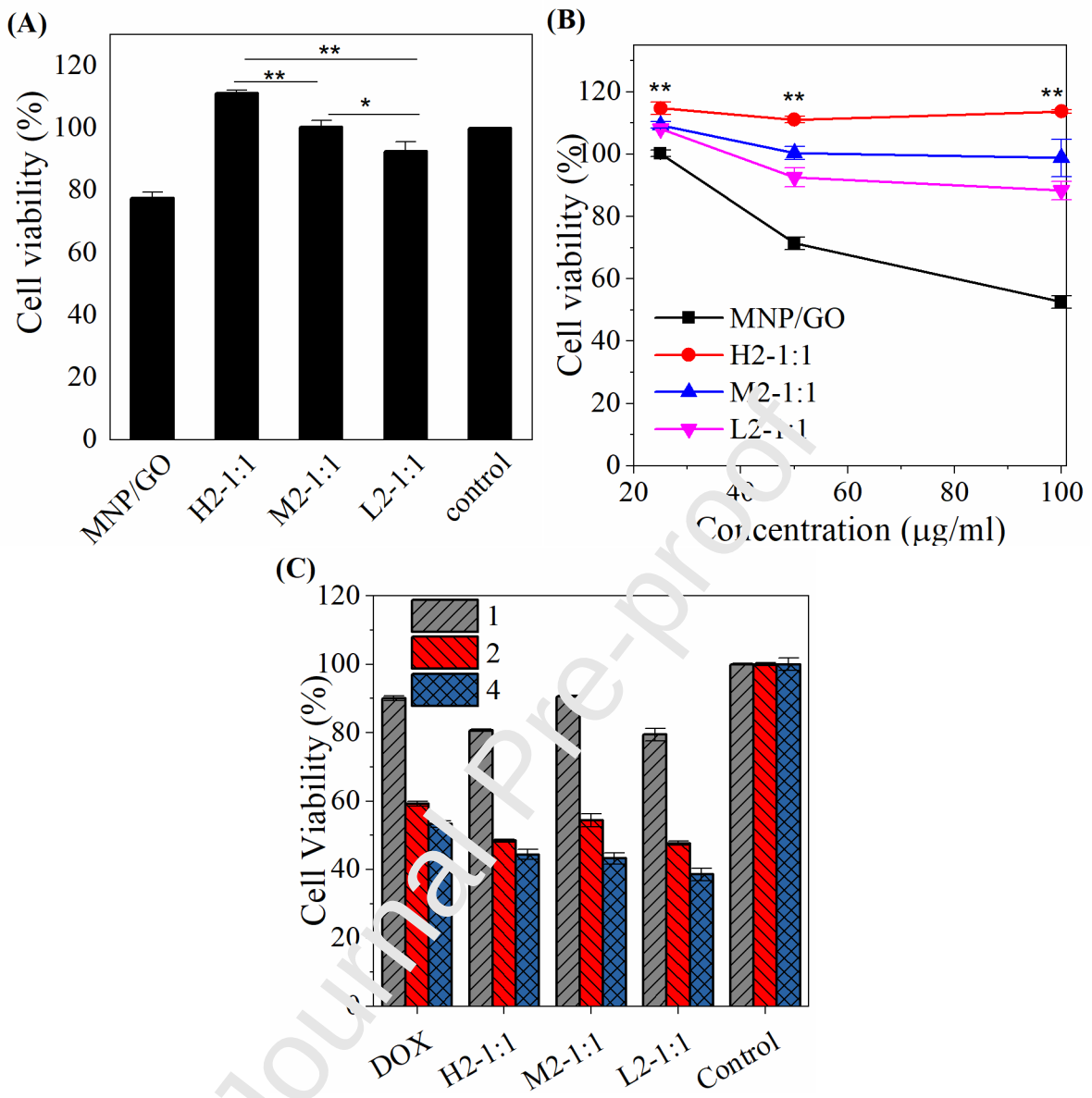

Fig. 5. Cell viability of L-929 cells under different treatments with the concentration of 50 µg/ml (A). Cell viability profile as a function of nano-system concentration for fibroblast cells of L-929 in MNP/GO, H2-1:1, M2-1:1 and L2-1:1 sample (*$p<0.05$ and ** $p<0.0001$) (B). MCF7 toxicity of different concentrations of doxorubicin-loaded samples (H2-1:1, M2-1:1 and L2-1:1) in three concentrations of Aliquot doxorubicin (1, 2 and 4 µg/ml). Doxorubicin and drug-free culture environment were chosen as the positive and negative controls, respectively (C).

3.6 Magnetic Properties

VSM measurements of field dependent magnetization for different nano-systems at constant temperature (**Fig. 6**) displayed superparamagnetic behavior with no hysteresis cycle, coercive field or remnant magnetization. The saturation magnetization (M_s) decreased for MNP/GO compared to pristine MNP and decreased by increasing the chitosan molecular weight. Through

agglomeration of MNPs, the magnetization can increase as a result of decrease in the surface coverage with surfactant or polymer as previously report [62], however the use of GO nano sheets for deposition of MNPs prevents them from agglomerating. In addition, an increasing on the molecular weight of chitosan can decrease the chance of agglomeration of the components via steric hinderance and electrostatic repulsion which is originated from their intrinsic positive charge of the chitosan chains.

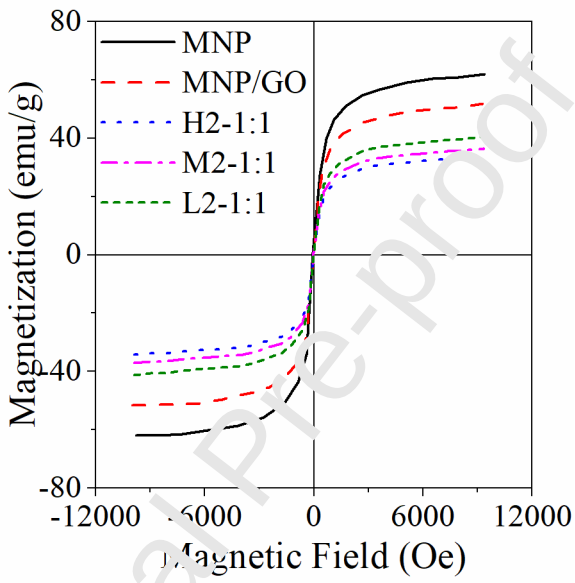

Fig. 6: Magnetization graph for MNPs, MNP/GO, L2-1:1, M2-1:1 and H2-1:1 sample at 25℃.

The R_1 relaxations of the samples depicted in **Fig. 7-A** showed a liner dependence of relaxation rates linear with iron concentrations for all samples, with the MNP/GO showing higher relaxivity (the slope of the R_1 vs. concentration) compared to pure MNP, whilst the addition of chitosan reduced R_1 relaxivity of the system. In addition, it was observed that increasing the molecular weight caused reduction in R_1 relaxivity. As mentioned previously in subsection 3-2 (**Fig. 2-A**), GO have several hydrophilic functional groups such as hydroxyl, carboxylic acid and epoxide, all having a potential for hydrogen bonding. Therefore, by modifying magnetic nanoparticles with GO, the number of hydrogen bonds between water and MNP increases, which in turn enhances the spin-lattice relaxation rate. Though chitosan has several hydrophilic agents, it is insoluble in water at pH=7.4; therefore, water penetration in the nanocomposite structure is not possible. By increasing the molecular weight, water penetration into the chitosan chains gets harder and R_1 relaxivity decreases [63].

Clustering of T_2 contrast agents is known as one of the main reasons of increasing R_2 relaxivity (the slope of the R_2 vs. concentration) in spin-spin relaxation mechanism. R_2 relaxation curves for different samples were represented in **Fig. 7-B**. Addition of GO and chitosan prevents MNPs from clustering, therefore r_2 relaxivity of the nano-systems decreases in comparison with bare,

unmodified MNPs. The reduction in r_2 relaxivity through increasing molecular weight resulted in an enhancement in the stability of the system, preventing agglomerate formation [64], highlight desirable for a theranostics delivery system.

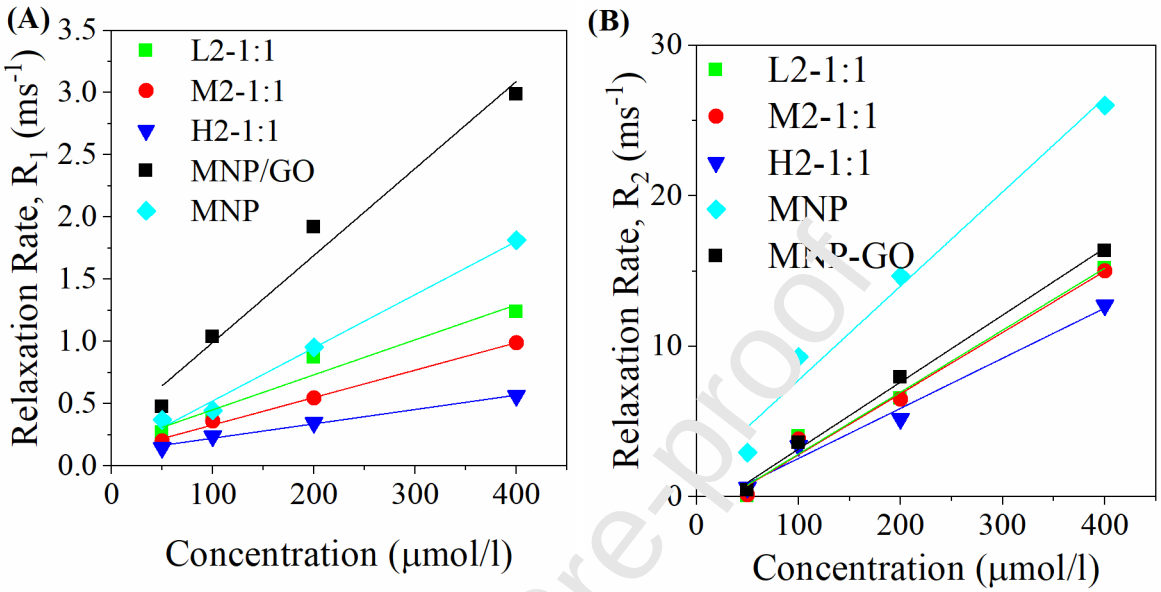

Fig. 7: $R_1 = 1/T_1$ (A) and $R_2 = 1/T_2$ (B) relaxation rates as a function of MNPs concentration for pure MNP, MNP/GO, L2-1:1, M2-1:1 and H2-1:1.

For T_2 contrast agents, the r_2/r_1 ratio gives information about contrast efficacy; the higher r_2/r_1 ratio means a better contrast efficacy. The r_1, r_2 and r_2/r_1 ratio of nano-systems were summarized in **Table 2,** and showed that though r_2 decreases by incorporating GO and chitosan into nano-system, the r_1 relaxivity reduced sharply to almost one seventh for H2-1:1 comparing with MNP/GO. It explains how T_2 contrast efficacy improved by introducing chitosan and GO. Despite the r_2 decrease, intense decrease in r_1 for these samples enhances the r_2/r_1 ratio, which resulted in the higher resolution of chitosan-grafted samples. H2-1:1 sample presented the highest resolution with r_2/r_1 value of 28.95.[75]

Table 2: MRI relaxivity results.

Sample Code	**r_1 (mM^{-1} s^{-1})**	**r_2 (mM^{-1} s^{-1})**	**r_2/r_1**
MNP	4.27	62.53	14.66
MNP/GO	6.99	44.51	6.37
L2-1:1	2.81	41.16	14.49

M2-1:1	2.20	40.68	18.49
H2-1:1	1.15	33.30	28.95

Recent studies reported theranostic systems based on water-soluble chitosan are not capable of being used as an active targeted system [65-66]. Some earlier studies have also reported the use of chitosan/GO nano systems but without optimizing performance in respect to drug loading, release, and magnetic behavior [47]. Out study shows, the chitosan MNP/GO system possesses efficient pH-sensitivity couple to maximum coverage of GO surface with enhancement in both drug loading and drug release. Among all nano-systems, sample containing high molecular weight chitosan and high concentration was on the overall the best, combining high T2 contrast, pH sensitivity, biocompatibility and drug loading good doxorubicin release profile and a cellular toxicity effect on cancerous cells.

4. Conclusion

The sparse grafting of the chitosan chains on GO surface results in a strong burst release of doxorubicin. Grafting of concentrated high molecular weight chitosan on MNP/GO caused good rates of release of doxorubicin linked to the full coverage of GO surface with chitosan chains. The use of high molecular weight chitosan for grafting MNP/GO also improved the total drug loading through more sites for drug/polymer complexation. The chitosan coating of MNP/GO reduced toxicity of the hybrid nano-system, overcoming one of the main limitations for clinical use of GO nanosheets. High molecular weight of chitosan allowed reducing toxicity, which can be desirable for applications involving healthy cells, yet for cancer drug delivery low molecular weight chitosan is preferred due to the higher amount of drug release. Study of the effect of GO and chitosan on magnetic behavior of the MNP/GO system showed GO decreased the contrast efficacy of the MNP, yet grafting of MNP/GO with hydrophobic chitosan enhanced the contrast efficacy as seen from the sharp decrease in r_1 relaxivity which is very desirable for MR imaging applications. Our study showed modification of MNP/GO nanocarriers with the pH-sensitive biocompatible chitosan allowed overcoming many limitations previously flagged in literature, opening up a number of applications of these advanced nano-systems for theranostic applications in the near future.

References

[1] Organization WH. World health statistics 2019: Monitoring health for the SDGs, sustainable development goals. 2019, 1-62.

[2] Greish K. Enhanced permeability and retention (EPR) effect for anticancer nanomedicine drug targeting. Cancer Nanotechnology. 2010 Jan 25; 25-37.

[3] Li X, Zhou H, Wu W, Wei S, Xu Y, Kuang Y. Studies of heavy metal ion adsorption on Chitosan/Sulfydryl-functionalized graphene oxide composites. Journal of Colloid and Interface Science. 2015 June 15; 448: 389-397.

[4] Peer D, Karp JM, Hong S, Farokhzad OC, Margalit R, Langer R. Nanocarriers as an emerging platform for cancer therapy. Nature Nanotechnology. 2007 Dec; 2: 751-760.

[5] Sahoo SK, Labhasetwar V. Nanotech approaches to drug delivery and imaging. Drug Discovery Today. 2003 Dec 15; 8(24):1112-1120.

[6] Cole JT, Holland NB. Multifunctional nanoparticles for use in theranostic applications. Drug Delivery and Translational Research volume. 2015 Feb 24; 5: 295-309.

[7] Li D, Kang J, Golas BJ, Yeung VW, Madoff DC. Minimally invasive local therapies for liver cancer. Cancer Biology and Medicine. 2014 Dec; (11)4: 217-236.

[8] Allemani C, Matsuda T, Carlo VD, Harewood R, Matz M, Nikšić M, Bonaventure A, Valkov PM, Johnson CJ, Estève J, JOgunbiyi O, AzevedoeSilva G, QingChen W, Eser S, Engholm G, Stiller CA, Monnereau A, Woods RR, Visser O, HsiangLim G, AitkenKWeir H, PColeman M. Global surveillance of trends in cancer survival 2000–14 (CONCORD-3): analysis of individual records for 37 513 025 patients diagnosed with one of 18 cancers from 322 population-based registries in 71 countries. The Lancet. 2018 March 17-23; 391(10125): 1023-1075.

[9] Sanna V, Pala N, Sechi M. Targeted therapy using nanotechnology: focus on cancer. International Journal of Nanomedicine. 2014 Jan 15; 9: 467-483.

[10] Makvandi P, Wang CY, Nazarzadeh Zare E, Borzacchiello A, Niu LN, Tay FR. Metal-Based Nanomaterials in Biomedical Applications: Antimicrobial Activity and Cytotoxicity Aspects. Advanced Functional Materials, 2020 Mar 17; 30(22).

[11] Liu F, Huang P, Huang D, Liu S, Cao Q, Dong X, Zhang H, Ko F, Zhou W. Smart "on-off" responsive drug delivery nanosystems for potential imaging diagnosis and targeted tumor therapy. Chemical Engineering Journal, 2019 June 1; 365: 358-368.

[12] Wang CY, Makvandi P, Nazarzadeh Zare E, Niu LN, Tay FR. Advances in Antimicrobial Organic and Inorganic Nanocompounds in Biomedicine.Advanced Therapeutics, 2020 May 27; 3(8).

[13] Jokerst JV, Gambhir SS. Molecular imaging with theranostic nanoparticles. Accounts of Chemical Research. 2011 Sep 15; 44(10):1050-1060.

[14] Chowdhuri AR, Laha D, Chandra S, Karmakar P, Sahu SK. Synthesis of multifunctional up conversion NMOFs for targeted antitumor drug delivery and imaging in triple negative breast cancer cells. Chemical Engineering Journal. 2017 Jul 01; 319: 200-211.

[15] Funkhouser J. Reinventing pharma: the theranostic revolution. Current Drug Discovery. 2002; 2: 17-19.

[16] Martin KH, Dayton PA. Current status and prospects for microbubbles in ultrasound theranostics. Wires Nanomedicine and Nanobiotechnology. 2013 Jul-Aug; 5(4): 329-345.

[17] Ragheb RRT, Kim D, Bandyopadhyay A, Chahboune H, Bulutoglu B, Ezaldein H, Criscione JM, Fahmy TM. Induced clustered nanoconfinement of superparamagnetic iron oxide in biodegradable nanoparticles enhances transverse relaxivity for targeted theranostics. Magnetic Resonance in Medicine. 2013 Dec; 70(6): 1748-1760.

[18] Pellico J, Ellis CM, Davis JJ. Nanoparticle-Based Paramagnetic Contrast Agents for Magnetic Resonance Imaging. Contrast Media & Molecular Imaging. 2019 May 05; 2019:1-13.

[19] Houssami N, Hayes DF. Review of preoperative magnetic resonance imaging (MRI) in breast cancer: should MRI be performed on all women with newly diagnosed, early stage breast cancer? CA: A Cancer Journal for Clinicians. 2009 Sep-Oct; 59(5): 290-302.

[20] Sanjai C, Kothari S, Gohil P, Saesoo S, Sajomsang W.Chitosan-triphosphate nanoparticles for encapsulation of super-paramagnetic iron oxide as an MRI contrast agent. Carbohydrate Polymers. 2014 Apr 15; 104: 231-237.

[21] Yang L, Wang Z, Ma L, Li A, Xin J, Wei R, Lin H, Wang R, Chen Z, Gao J. The roles of morphology on the relaxation rates of magnetic nanoparticles. ACS Nano. 2018 Apr 19; 12(5): 4605-4614.

[22] Lin BR, Chen CH, Kunuku S, Chen TY, Hsiao TY, Niu H, Lee CP, Fe doped magnetic nanodiamonds made by ion implantation as contrast agent for MRI, Scientific Reports. 2018 May 04; 8(7058): 1-6.

[23] Stoll S, Mertzman J, VanKeuren E, Albanese C, Fricke S. Manganese-oxo clusters as contrast agents for magnetic resonance imaging. Patent. (US10342881B2) 2019.

[24] Bao Y, Sherwood J, Sun Z. Magnetic iron oxide nanoparticles as T1 contrast agents for magnetic resonance imaging. Journal of Materials Chemistry C. 2018 Jan 15; 6(6): 1280-1290.

[25] Upponi JR, Jerajani K, Nagesha DK, Kulkarni P, Sridhar S, Ferris C, Torchilin VP. Polymeric micelles: Theranostic co-delivery system for poorly water-soluble drugs and contrast agents. Biomaterials. 2018 Jul; 170: 26-36.

[26] Wang FH, Bae K, Huangb ZW, Xue JM, Two-photon graphene quantum dot modified Gd $_2O_3$ nanocomposites as a dual-mode MRI contrast agent and cell labelling agent. Nanoscale.2018 Feb 16; 10(12): 5642-5649.

[27] Chen L, Zang F, Wu H, Li J, Xie J, Ma M, Gu N, Zhang Y. Using PEGylated magnetic nanoparticles to describe the EPR effect in tumor for predicting therapeutic efficacy of micelle drugs. Nanoscale. 2018 Dec 21; 10(4): 1788-1797.

[28] Chen J, Wang X, Liu Y, Liu H, Gao F, Lan C, Yang B, Zhang S, Gao Y. pH-responsive catalytic mesocrystals for chemodynamic therapy via ultrasound-assisted Fenton reaction. Chemical Engineering Journal. 2019 Aug 01; 369: 394-402.

[29] Xing XJ, Xiao WL, Liu XG, Zhou Y, Pang DW, Tang HW. A fluorescent aptasensor using double-stranded DNA/graphene oxide as the indicator probe. Biosensors and Bioelectronics. 2016 Apr 15; 78: 431-437.

[30] Cui X, Dong L, Zhong S, Shi C, Sun Y, Chen P. Sonochemical fabrication of folic acid functionalized multistimuli-responsive magnetic graphene oxide-based nanocapsules for targeted drug delivery. Chemical Engineering Journal. 2017 Oct 15; 326: 839-848.

[31] Wang G, Ma Y, Wei Z, Qi M. Development of multifunctional cobalt ferrite/graphene oxide nanocomposites for magnetic resonance imaging and controlled drug delivery. Chemical Engineering Journal. 2016 Apr 01; 289: 150-160.

[32] Wang N, Lin M, Dai H, Wang HMa. Functionalized gold nanoparticles/reduced graphene oxide nanocomposites for ultrasensitive electrochemical sensing of mercury ions based on thymine–mercury–thymine structure. Biosensors and Bioelectronics. 2016 May 15; 79:320-326.

[33] Park S, Mohanty N, Suk JW, Nagaraja A, An J, Piner RD, Cai W, Dreyer DR, Berry V, Ruoff RS. Biocompatible, robust free- standing paper composed of a TWEEN/graphene composite. Advanced Materials. 2010 Apr 18; 22(15):1736-1740.

[34] Pramanik N, Ranganathan S, Rao S, Suneet K, Jain S, Rangarajan A, Jhunjhunwala SA. Composite of Hyaluronic Acid-Modified Graphene Oxide and Iron Oxide Nanoparticles for Targeted Drug Delivery and Magnetothermal Therapy. ACS Omega. 2019 28 May; 4(5): 9284-9293.

[35] Kim H, Tator CH, Shoichet MS. Chitosan implants in the rat spinal cord: biocompatibility and biodegradation. Journal of Biomedical Materials Research Part A. 2011 Apr 04;97(4)395-404.

[36] Dragostin OM, Samal SK, Dash M, Lupascu F, Pânzariu A, Tuchilus C, Ghetue N, Dubruel P, Pieptu D, Vasile C, Tatia R, Profire L. New antimicrobial chitosan derivatives for wound dressing applications. Carbohydrate Polymers. 2016 May 05; 141: 28-40.

[37] Niu S, Williams GR, Wu J, Wu J, Zhang X, Zheng H, Lee S, Zhu LM. A novel chitosan-based nanomedicine for multi-drug resistant breast cancer therapy. Chemical Engineering Journal. 2019 Aug 01; 369:134-149.

[38] Daeil C, Sangmin J, Dong CY, Wooram U, Jeong YK, Hong YY, Hyeyoun C, Dong EK, Jae HP, Hyuncheol K, Kwangmeyung K. Iodinated echogenic glycol chitosan nanoparticles for X-ray CT/US dual imaging of tumor. Nanotheranostics.2018 Jan 01;2(2): 117-127.[39] Mianehrow H, Afshari R, Mazinani S, Sharif FM. introducing a highly dispersed reduced graphene oxide nano-biohybrid employing chitosan/hydroxyethyl cellulose for controlled drug delivery. International Journal of Pharmaceutics. 2016 Jul 25; 509(1-2):400-407.

[40] Wang C, Chen,B, Zou M, Cheng G. Cyclic RGD-modified chitosan/graphene oxide polymers for drug delivery and cellular imaging. Colloids and Surfaces B: Biointerfaces.2014 Oct 01; 122: 332-340.

[41] Pan Y, Wu T, Bao H, Li L. Green fabrication of chitosan films reinforced with parallel aligned graphene oxide. Carbohydrate Polymers. 2011 Feb 01; 83(4)1908-1915.

[42] Yang X, Tu Y, Li L, Shang S, Tao X. Well-dispersed chitosan/graphene oxide nanocomposites. ACS Applied Materials & Interfaces. 2010 Jun 07;2(6):1707-1713.

[43] Stankovich S, Dikin DA, Dommett GHB, Kohlhaas KM, Zimney EJ, Stach EA, Piner RD, Nguyen SBT, Ruoff RS. Graphene-based composite materials. Nature. 2006 Jul 20; 442 (7100):282-286.

[44] Han Q, Wang Z, Xia J, Chen S, Zhang X, Ding M. Facile and tunable fabrication of Fe3O4/graphene oxide nanocomposites and their application in the magnetic solid-phase extraction of polycyclic aromatic hydrocarbons from environmental water samples. Talanta. 2012 Nov 15; 101: 388-395.

[45] Yang Y, Wang J, Zhang J, Liu J, Yang X, Zhao H. Exfoliated graphite oxide decorated by PDMAEMA chains and polymer particles. Langmuir. 2009 Jul 14; 25(19):11808-11814.

[46] Yang K, Zhang S, Zhang G, Sun X, Lee ST, Liu Z. Graphene in mice: ultrahigh in vivo tumor uptake and efficient photothermal therapy. Nano letters. 2010 Aug 04; 10(9): 3318-3323.

[47] Wang C, Ravi S, Garapati US, Das M, Howell M, Mallela J, Alwarappan S, Mohapatra SS, Mohapatra S. Multifunctional chitosan magnetic-graphene (CMG) nanoparticles: a theranostic platform for tumor-targeted co-delivery of drugs, genes and MRI contrast agents. Journal of Materials Chemistry B. 2013 Jun 17; 1(35): 4396-4405.

[48] Schmaljohann D. Thermo- and pH-responsive polymers in drug delivery. Advanced Drug Delivery Reviews. 2006 Dec 30; 58(15):1655-1670.

[49] Liu J, Huang Y, Kumar A, Tan A, Jin S, Mozhi A, Liang XJ. pH-sensitive nano-systems for drug delivery in cancer therapy. Biotechnology Advances. 2014 Jul-Aug; 32(4):693-710.

[50] Cho Y, Kim H, Choi Y. A graphene oxide–photosensitizer complex as an enzyme-activatable theranostic agent. Chemical Communications. 2012 Dec 18; 49(12):1202-1204.

[51] Dresco PA, Zaitsev VS, Gambino RJ, Chu B. Preparation and properties of magnetite and polymer magnetite nanoparticles. Langmuir. 1999 17 Feb; 15(6):1945-1951.

[52] Stobinski L, Lesiak B, Malolepszy A, Mazurkiewicz M, Mierzwa B, Zemek J, Jiricek P, Bieloshapkad I. Graphene oxide and reduced graphene oxide studied by the XRD, TEM and

electron spectroscopy methods. Journal of Electron Spectroscopy and Related Phenomena. 2014 Aug; 195:145-154.

[53] Park S, An J, Potts JR, Velamakanni A, Murali S, Ruoff RS. Hydrazine-reduction of graphite-and graphene oxide. Carbon. 2011 Aug; 49(9):3019-3023.

[54] Kasaai MR. A review of several reported procedures to determine the degree of N-acetylation for chitin and chitosan using infrared spectroscopy. Carbohydrate Polymers. 2008 Mar 07; 71(4): 497-508.

[55] Corazzari I, Nisticò R, Turci F, Faga MG, Franzoso F, Tabasso S, Magnacca G. Advanced physico-chemical characterization of chitosan by means of TGA coupled on-line with FTIR and GCMS: Thermal degradation and water adsorption capacity. Polymer Degradation and Stability.2015 Feb; (112):1-9.

[56] Hu H, Wang X, Wang J, Liu F, Zhang M, Xu C. Microwave-assisted covalent modification of graphene nanosheets with chitosan and its electrorheological characteristics. Applied Surface Science. 2011 Jan 15; 257(7): 2637-2642.

[57] Farazi R, Vaezi MR, Molaei MJ, Saeidifar M, Behnam-Ghader AA. Effect of pH and temperature on doxorubicin hydrochloride release from magnetite/graphene oxide nanocomposites. Materials Today Proceeding.2018 Jun 08; 5(7)(3): 15726-15732.

[58] Kayitmazer AB, Strand SP, Tribet C, Jaeger W, Dubin PL. Effect of polyelectrolyte structure on protein− polyelectrolyte coacervates: Coacervates of bovine serum albumin with poly (diallyldimethylammonium chloride) versus chitosan. Biomacromolecules. 2007 25 Sep; 8(11): 3568-3577.

[59] Sanyakamdhorn S, Agudelo D, Tajmir-Riahi HA. Encapsulation of antitumor drug doxorubicin and its analogue by chitosan nanoparticles. Biomacromolecules. 2013 Jan 10; 14(2):557-563.

[60] Wojtoniszak M, Chen X, Kalenczuk RJ, Wajda A, Lapczuk J, Kurzewski M, Drozdzik M, Chu PK, Palen EB. Synthesis, dispersion, and cytocompatibility of graphene oxide and reduced graphene oxide. Colloids and Surfaces B: Biointerfaces. 2012 Jan 01; (89):79-85.

[61] Chowdhuri AR, Singh T, Ghosh SK, KumarSahu S. Carbon dots embedded magnetic nanoparticles@ chitosan@ metal organic framework as a nanoprobe for pH sensitive targeted anticancer drug delivery. ACS Applied Materials & Interfaces. 2016 Jun 15; 8(26):16573-16583.

[62] Lee HS, Shao H, Huang Y, Kwak B. Synthesis of MRI contrast agent by coating superparamagnetic iron oxide with chitosan. IEEE Transactions on Magnetics. 2005 Oct; 41(10): 4102-4104.

[63] Wang Y, Ngy W, Chen Y, Shuter B, Yi J, Ding J, Wang SC, Feng SS. Formulation of superparamagnetic iron oxides by nanoparticles of biodegradable polymers for magnetic resonance imaging. Advanced Functional Materials. 2008 Jan ;18(2): 308-318.

[64] Qin J, Laurent S, Jo YS, Roch A, Mikhaylova M, Bhujwalla ZM, Muller RN, Muhammed M. A high- performance magnetic resonance imaging T2 contrast agent. Advanced Materials.2007 Jul 06 ;19(4):1874-1878.

[65] Roshidi MDA, Fen YW, Omar NAS, Saleviter S, Daniyal WMEMM. Optical Studies of Graphene Oxide/poly (amidoamine) Dendrimer Composite Thin Film and Its Potential for Sensing Hg2+ Using Surface Plasmon Resonance Spectroscopy. Sensors and Materials. 2019 Oct ;31(4) (2019):1147-1156.

[66] Zhang H, Yan T, Xu S, Feng S, Huang D, Fujita M, Jao XD. Graphene oxide-chitosan nanocomposites for intracellular delivery of immunostimulatory CpG oligodeoxynucleotides. Materials Science and Engineering: C. 2017 Apr 01;73:144-151.

|Supporting Information|

Development and Optimization of a New Hybrid Chitosan-grafted Graphene Oxide/Magnetic Nanoparticle System for Theranostic Applications

M. Saviz Baktash[1], Ali Zarrabi [1,2*], Ehsan Avazverdi[3], Nuno Miguel Reis[4]

[1] Department of Biotechnology, Faculty of Biological Science and Technology, University of Isfahan, Isfahan, Iran
[2] Sabanci University Nanotechnology Research and Application Center (SUNUM), Tuzla 34956, Istanbul, Turkey
[3] Department of Polymer Engineering and Color Technology (Tehran Polytechnic), No.350, Hafez Ave., Tehran, Iran
[4]Centre for Biosensors, Bioelectronics and Biodevices (C3Bio) and Department of Chemical Engineering, University of Bath, Claverton Down, Bath BA2 7AY, United Kingdom

Determination of critical concentrations

In order to determine the C* (chain overlap concentration) and C** (the concentration that beyond which the concentration fluctuations become weak[1], rheological assessments were carried out. chitosan solutions with high, medium and low molecular weight were prepared in 1.8% v/v acetic acid solution. The concentration ranges of the chitosan solutions were chosen between 0.25 to 6 % w/v. The rotational mode of the steady shear rate sweep test was performed by a cone and plate rheometer (MCR301, Anton Paar, Austria). The cone angle and diameter were equal to 2° and 25 mm, respectively. Test was carried out at a constant temperature of 25°C with the scanned shear rates in the range of 0.01 to 200 s^{-1}. The specific zero shear viscosity were calculated as follow:

Chitosan concentration ranges

The specific shear viscosity versus shear rate at various concentrations of chitosan with three different molecular weights have been illustrated in Figure S1(A-C). The viscosity of the polymeric solution is shifted to higher values by increasing the chitosan molecular weight. Moreover, for all three molecular weights in diluted solutions (less than 0.5% w/v), the viscosity was constant by increasing the shear rate, suggesting a Newtonian behavior at low concentrations; however, at concentrations above 0.5% w/v, the shear thinning behavior was observed. This behavior was more significant at concentrations higher than 2.5% w/v. Due to the absence of entanglements in dilute solutions, the viscosity shows a plateau in wide viscosity ranges. While in semi-concentrated and concentrated systems, the response of each chitosan chain to the shear is affected by the neighboring chains. Especially in concentrated systems, the change from Newtonian to non-Newtonian behavior was clearly observed due to the interlocking of chitosan chains. As the chitosan concentration was increased, the length of the Newtonian region decreased and finally vanished at concentrated solutions. The probability of inter-chain

* Corresponding author, E-mail: alizarrabi@sabanciuniv.edu
Tel: 0090 216 4839666, Fax: 0090 216 4839118

entanglement enhanced by increasing the number of chitosan chains in a constant volume of the solution; hence, the applied shear stress is propagated between chitosan chains; therefore, even very low shear rates may contribute to the deformation of polymer chains.

Variations in the specific zero-shear viscosity (η_{0sp}) versus concentration for low, medium and high molecular weight chitosan was shown in Figure S1-D in a logarithmic scale. As it can be observed, increasing concentration, the specific zero-shear viscosity remained mostly constant, then increased gently and finally rose sharply. The response of the specific zero-shear viscosity to concentration for each chitosan molecular weight could be categorized in three regions:

- Diluted region (below C*): where the specific zero-shear viscosity is almost independent to the concentration, and inter-chain interactions can be neglected, assuming an independent behavior for each chain.

- Semi-concentrated region (between C* and C**): where, the specific zero-shear viscosity was a function of the concentration. In other words, hydrodynamic spheres of the chains are in contact with each other.

- Concentrated region (above C**): in this region, the slope of the logarithmic specific zero-shear viscosity versus logarithmic concentration increases rapidly and hydrodynamic spheres of the chains are merged into each other and the chain entanglement is imminent.

The extracted results of the Figure S1-D are summarized in Table S1. The points at which the first and second slope changes have occurred can be considered as C* and C**, respectively. As it was expected, by increasing the molecular weight, C** shifted to lower concentrations while the C* did not significantly change.

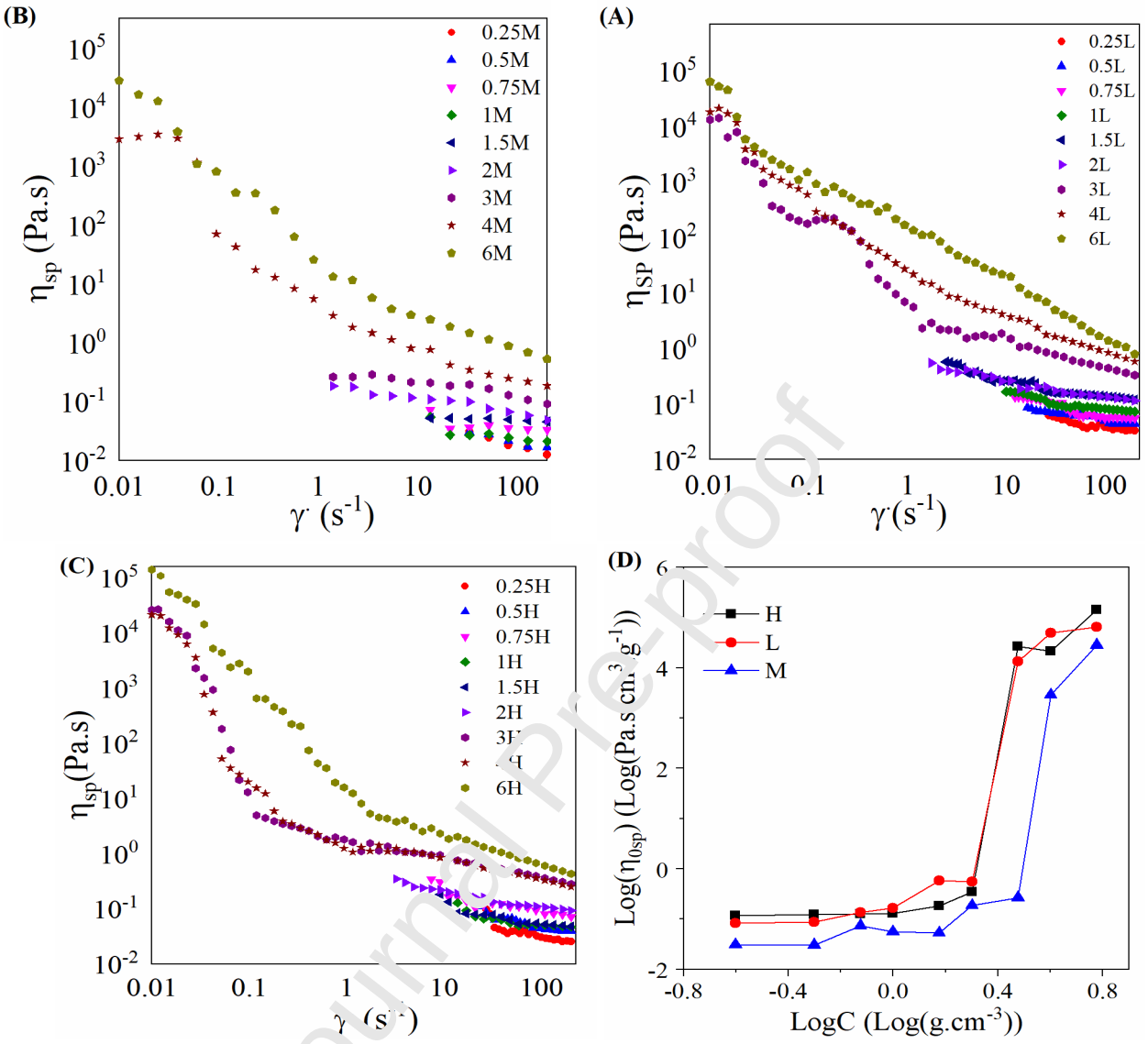

Fig.S1: The specific shear viscosity for low (A), medium (B) and high (C) molecular weight chitosan solutions in different concentrations. The specific zero-shear viscosity changes versus concentrations for low, medium and high molecular weight chitosan solutions (D).

Table S1. Data extracted from Figure S1-D for each chitosan molecular weight

Chitosan Type	First Regime			Second Regime			Third Regime		
	concentration Range (g/ml)	Slope	Adjusted R-square	concentration Range (g/ml)	Slope	Adjusted R-square	concentration Range(g/ml)	Slope	Adjusted R-square
High molecular weight	0.25-0.5	0.077	1	0.5-2	0.95	0.68	2-6	14.25	0.84
Medium molecular weight	0.25-5	-0.01	1	0.5-3	1.3	0.72	3-6	15.9	0.64
Low molecular weight	0.25-0.5	0.03	1	0.5-2	1.49	0.89	2-6	10.22	0.58

Supplementary References

[1] Muthukumar M, A perspective on polyelectrolyte solutions. Macromolecules, 50th anniversary perspective. 2014 Dec 14; 50(24): 528-9560.

Author statement:

M. Saviz Baktash: Investigation, Writing- Original draft

Ali Zarrabi: Project administration, Supervision, Writing - Review & Editing

Ehsan Avazverdi: Conceptualization, Methodology, Validation

Nuno Miguel Reis: Supervision, Writing - Review & Editing, Data Curation

Declaration of interests

☒ The authors declare that they have no known competing financial interests or personal relationships that could have appeared to influence the work reported in this paper.

☐The authors declare the following financial interests/personal relationships which may be considered as potential competing interests:

Graphical abstract

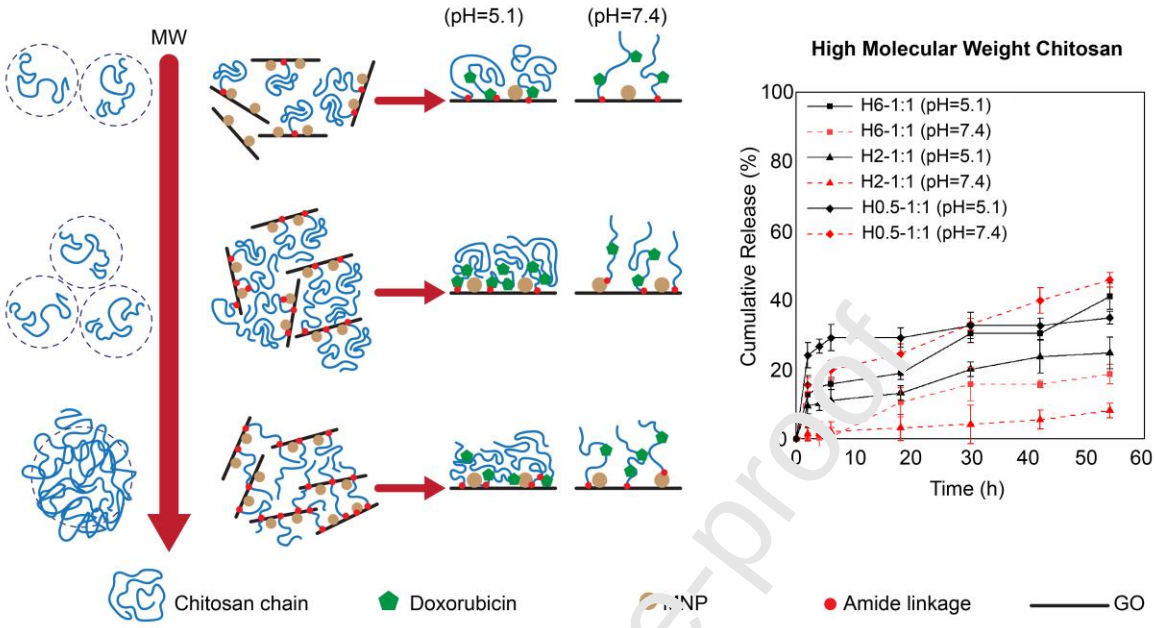

Development and Optimization of a New Hybrid Chitosan-grafted Graphene Oxide/Magnetic Nanoparticle System for Theranostic Applications

M. Saviz Baktash[1], Ali Zarrabi [1,2*], Ehsan Avazverdi[3], Nuno Miguel Reis[4]

[1] Department of Biotechnology, Faculty Biological Sciences and Technologies, University of Isfahan, Isfahan, Iran
[2] Sabanci University Nanotechnology Research and Application Center (SUNUM), Tuzla 34956, Istanbul, Turkey
[3] Department of Polymer Engineering and Color Technology (Tehran Polytechnic), No.350, Hafez Ave., Tehran, Iran
[4] Centre for Biosensors, Bioelectronics and Biodevices (C3Bio) and Department of Chemical Engineering, University of Bath, Claverton Down, Bath BA2 7AY, United Kingdom

Highlights

- Modifying GO with high molecular weight chitosan improves its biocompatibility.
- Weight and concentration have strong impact on drug release from the nano-system.
- Sparse grafting of chitosan causes strong burst drug release and weak pH-dependency.
- Chitosan hydrogen bonds with water molecules enhances T2 contrast.

* Corresponding author, E-mails: alizarrabi@sabanciuniv.edu
Tel: 0090 216 4839666, Fax: 0090 216 4839118